International Core Journal of Engineering Volume 7 Issue 5, 2021
ISSN: 2414-1895 DOI: 10.6919/ICJE.202105_7(5).0060

Design of Double-stator PMSM based Propulsion System with Energy Recovery for Electric Aircraft

Chunjie Dai

Logistics Engineering College, Shanghai Maritime University, Shanghai 201306, China.

daichunjie@stu.shmtu.edu.cn

Abstract

This paper presents an electric propulsion system (EPS) based on double-stator permanent magnet synchronous machine (DSPMSM) for an electric aircraft (EA). In the system, DSPMSM and propeller are modelled in detail. The control scheme in traction and generator mode is studied. Maximum power point track (MPPT) algorithm is applied in the generator mode to increases the efficiency of energy recovery. The effectiveness of system modelling and control algorithm is verified in the MATLAB/Simulink simulation.

Keywords

Double-stator PMSM; Electric Aircraft; Energy Recovery; MPPT; Field-oriented Control.

1. Introduction

Environmental issue has become a topic that human society cannot avoid at present. Although air passenger traffic has increased rapidly and has made global transportation more convenient, it also remains costly and accounts for around 2% of greenhouse gas (GHG) emissions [1]. Therefore, the state-of-the-art on-board systems are requested to be safer, quitter, more efficient and environmentally friendly. A more electric aircraft (MEA) or all electric aircraft (AEA) is proposed to meet these requirements [2-4]. The conventional mechanical, hydraulic and pneumatic systems are replaced with electrical counterparts in an AEA. As a result, the design of electrical propulsive system of AEA is especially important and determines the performance of AEA to a large extent. Among many kinds of AEAs, ultra-light aircraft (ULA) or very light aircraft (VLA) is the research object in this paper because of its higher efficiency and usage value. In recent years, a growing interest in multiphase permanent magnet synchronous machine (PMSM) has risen due to their high performance, such as the ability of redundancy design and fault-tolerance structure [5], reduced phase current and torque ripple , improved power density and reliability of the system [6]. With the development of permanent magnet materials, multiphase PMSM has been widely used in electric aircraft [1,7]. Among these multiphase machines, dual three phase or double-stator PMSM (DSPMSM) is a favoured choice for general aerospace application, striking a balance between necessary redundancy and undue complexity, while maintaining a balanced operation following a failure [1]. Therefore, DSPMSM is the main driving motor of the system in this study.

The improvement of efficiency of electrical propulsion system is crucial to the overall system efficiency due to the limitations of battery storage system technology. To address this problem, some researchers are focusing on increasing the energy density of battery material or optimizing the battery manage system (BMS) to improve the performance [8]. Some are aiming at optimizing the existing motor structure to pursue a lower losses and higher reliability [9-11]. Some are treating this issue in a higher perspective. Since existing overall system structure design of aircraft is based on traditional internal combustion engine propulsion, it is necessary to propose a new electrical power system

ISSN: 2414-1895 DOI: 10.6919/ICJE.202105_7(5).0060

according to the electrical characteristics of PMSM [12,13]. Though researchers are addressing this problem in different aspects, seldom paper considers to recovery energy from propeller during suitable situation like the regeneration braking techniques used in electric vehicles. As a result, this paper proposed a strategy to recover kinetic energy from propeller during landing phase. Propeller is treated as a wind turbine and kinetic energy is feedback to energy storage system through PMSM which is working in the generation mode in the period [14]. Maximum power point tracking (MPPT) algorithm is applied to seeking the optimal working point, thus the overall working efficiency can be improved with the strategy.

This paper is organized as follow: the overall system structure is illustrated in section 2 including modelling of DSPMSM and propeller. Section 3 introduces the control scheme of the system. Field-oriented control (FOC) is applied in torque control of DSPMSM. And MPPT algorithm is presented in this section. Simulation results are discussed in section 4, and conclusions are elaborated in the last section.

2. Modelling of the electric propulsion system

2.1 Description of the overall system

The overall structure diagram of EPS is shown in the figure 1. The system consists energy storage system, DC/DC converter, DC/AC inverter, DSPMSM, propeller and controller. As the main propulsive device of VLA, propeller provides thrust to drive the aircraft, which is directly driven by DSPMSM. And the motor is fed by two parallel three-phase AC power supplies inverted from DC link. Inverters connected with energy storage system via bidirectional DC/DC convertors, so that electrical energy generated by DSPMSM can feedback to energy storage system during landing. All these processes are under the control of controller. It acquires different signals from propeller, motor and other components. With necessary information, controller produces PWM signals to drive the switches in the converter and inverter. Working states can be monitored at the same time. In this study, we are focusing on the modelling of DSPMSM and the main control scheme including FOC and energy recovery method during landing

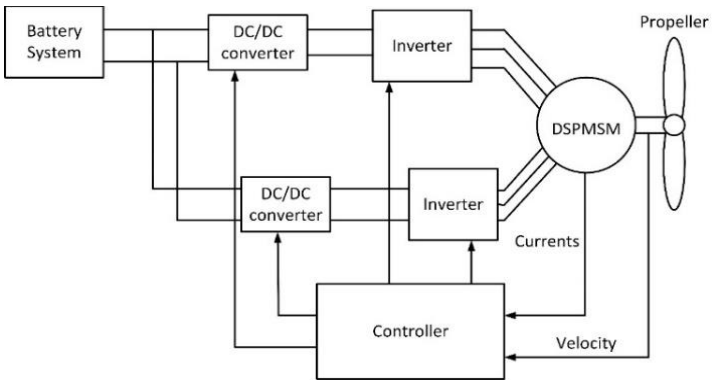

Figure 1. The overall structure diagram of EPS

2.2 Modelling of DSPMSM

In this section, the mathematic model of DSPMSM is described in three-phase static coordinate system. Then it can be developed into *d-q* rotating frame by applying Clack and Park transformation.

For a double-stator PMSM, each stator is a three-phase symmetrical winding. As a result, DSPMSM can be treat as a dual three-phase PMSM. The stators frame under different coordinate systems is presented in figure 2. Where a_1, b_1, c_1 and a_2, b_2, c_2 represent the first and second three-phase stator winding respectively. γ is the electrical angle between two stators. θ_1 and θ_2 are the electrical angle between *d*-axis with axis a_1, a_2. Two stators are rotating anti-clock wisely with the same electrical angular velocity ω.

ISSN: 2414-1895 DOI: 10.6919/ICJE.202105_7(5).0060

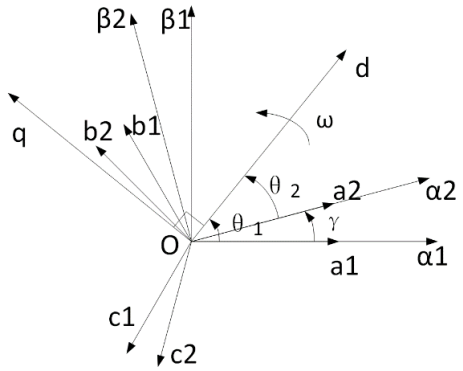

Figure 2. Coordinate diagram of DSPMSM in stationary and rotary reference frame

The voltage and flux linkage equations in three-phase coordinate system can be written as

$$u_{s1} = R_s i_{s1} + \frac{d}{dt}\varphi_{s1} \tag{1}$$

$$u_{s2} = R_s i_{s2} + \frac{d}{dt}\varphi_{s2} \tag{2}$$

$$\varphi_{s1} = L_{s1} i_{s1} + M_{s1s2} i_{s2} + \psi_{m1} \tag{3}$$

$$\varphi_{s2} = L_{s2} i_{s2} + M_{s1s2}^T i_{s1} + \psi_{m2} \tag{4}$$

where *Rs* is the stator resistance, u_{s1}, u_{s2}, i_{s1}, i_{s2} are the stator voltage and current vectors of two stators respectively. φ_{s1}, φ_{s2} are the stator flux linkage vectors. And they are defined as follow:

$$\mathbf{u_{s1}} = [u_{A1} \quad u_{B1} \quad u_{C1}]^T,\ \mathbf{u_{s2}} = [u_{A2} \quad u_{B2} \quad u_{C2}]^T,$$
$$\mathbf{i_{s1}} = [i_{A1} \quad i_{B1} \quad i_{C1}]^T,\ \mathbf{i_{s2}} = [i_{A2} \quad i_{B2} \quad i_{C2}]^T$$
$$\boldsymbol{\psi_{s1}} = [\psi_{A1} \quad \psi_{B1} \quad \psi_{C1}]^T, \boldsymbol{\psi_{s2}} = [\psi_{A2} \quad \psi_{B2} \quad \psi_{C2}]^T$$

$\boldsymbol{L_{s1}}$, $\boldsymbol{L_{s2}}$ are the inductance matrix of two stators. $\boldsymbol{M_{s1s2}}$ is the mutual inductance between two stators. $\boldsymbol{\psi_{m1}}$, $\boldsymbol{\psi_{m2}}$ are the flux linkage in the stator produced by permanent magnet. They are detailed in Appendix A

In order to obtain better dynamic performance like DC motor, coordinate transformation is applied to DSPMSM. By ignoring zero sequence component, DSPMSM can be represented as two three-phase motor with magnetic coupling through Clark and Park transformation [15].

$$[f_{Ax} \quad f_{Bx} \quad f_{Cx}]^T = T_{32}[f_{\alpha x} \quad f_{\beta x}]^T \tag{5}$$

$$[f_{\alpha x} \quad f_{\beta x}]^T = P(\theta_x)[f_{dx} \quad f_{qx}]^T \tag{6}$$

$$T_{32} = \sqrt{\frac{2}{3}}\begin{bmatrix} 1 & 0 \\ -\frac{1}{2} & \frac{\sqrt{3}}{2} \\ -\frac{1}{2} & -\frac{\sqrt{3}}{2} \end{bmatrix} \tag{7}$$

$$P(\theta_x) = \begin{bmatrix} cos\theta_x & -sin\theta_x \\ sin\theta_x & cos\theta_x \end{bmatrix} \tag{8}$$

where *f* represents electromagnetic variable such as voltage, current and flux linkage, *x* is the number of stators which can be 1,2 and T32, P(θ_x) are the Clark and Park transformation matrix.

The flux linkage and voltage expressions of DSPMSM in *d-q* frame can be deduced by applying transformation:

$$\begin{bmatrix} \psi_{1d} \\ \psi_{1q} \end{bmatrix} = \begin{bmatrix} L_{1d} & 0 \\ 0 & L_{1q} \end{bmatrix}\begin{bmatrix} i_{1d} \\ i_{1q} \end{bmatrix} + \begin{bmatrix} M_d & 0 \\ 0 & M_q \end{bmatrix}\begin{bmatrix} i_{2d} \\ i_{2q} \end{bmatrix} + \begin{bmatrix} \psi_{PM1} \\ 0 \end{bmatrix} \tag{9}$$

$$\begin{bmatrix} \psi_{2d} \\ \psi_{2q} \end{bmatrix} = \begin{bmatrix} L_{2d} & 0 \\ 0 & L_{2q} \end{bmatrix}\begin{bmatrix} i_{2d} \\ i_{2q} \end{bmatrix} + \begin{bmatrix} M_d & 0 \\ 0 & M_q \end{bmatrix}\begin{bmatrix} i_{1d} \\ i_{1q} \end{bmatrix} + \begin{bmatrix} \psi_{PM2} \\ 0 \end{bmatrix} \tag{10}$$

ISSN: 2414-1895 DOI: 10.6919/ICJE.202105_7(5).0060

$$\begin{bmatrix} u_{1d} \\ u_{1q} \end{bmatrix} = \begin{bmatrix} R_s + L_{1d} \cdot s & -\omega L_{1q} \\ \omega L_{1d} & R_s + L_{1q} \cdot s \end{bmatrix} \begin{bmatrix} i_{1d} \\ i_{1q} \end{bmatrix} + \begin{bmatrix} M_d \cdot s & -\omega M_q \\ \omega M_d & M_q \cdot s \end{bmatrix} \begin{bmatrix} i_{2d} \\ i_{2q} \end{bmatrix} + \begin{bmatrix} 0 \\ \omega \psi_{PM1} \end{bmatrix} \quad (11)$$

$$\begin{bmatrix} u_{2d} \\ u_{2q} \end{bmatrix} = \begin{bmatrix} R_s + L_{2d} \cdot s & -\omega L_{2q} \\ \omega L_{2d} & R_s + L_{2q} \cdot s \end{bmatrix} \begin{bmatrix} i_{2d} \\ i_{2q} \end{bmatrix} + \begin{bmatrix} M_d \cdot s & -\omega M_q \\ \omega M_d & M_q \cdot s \end{bmatrix} \begin{bmatrix} i_{s1d} \\ i_{s1q} \end{bmatrix} + \begin{bmatrix} 0 \\ \omega \psi_{PM2} \end{bmatrix} \quad (12)$$

where ω is the electrical angular speed, s is the differential operator,

$$L_{s1d} = L_1 - M_1 + \frac{3}{2}L_{12},\ L_{s2d} = L_2 - M_2 + \frac{3}{2}L_{22}$$

$$L_{s1q} = L_1 - M_1 - \frac{3}{2}L_{12},\ L_{s2q} = L_2 - M_2 - \frac{3}{2}L_{12},$$

$$\psi_{PM1} = \sqrt{\frac{3}{2}}\psi_{sm1},\ \psi_{PM2} = \sqrt{\frac{3}{2}}\psi_{sm2}$$

$$M_d = M_q = \frac{3}{2}M_0$$

The electromagnetic torque of DSPMSM can be estimated by using the sum of the cross product of the stator current vector and the flux linkage of both winding sets [16]. Assume that $L_{1d} = L_{2d} = L_d$, $L_{1q} = L_{2q} = L_q$ Hence, the electromagnetic torque of DSPMSM can be expressed as

$$T_e = p(\psi_{PM1} i_{1q} + \psi_{PM2} i_{2q} + (L_d - L_q)(i_{1d} i_{1q} + i_{2d} i_{2q}) + (M_d - M_q)(i_{1d} i_{2q} + i_{2d} i_{1q})) \quad (13)$$

where p is the number of pole pairs.

The mechanical equation is given as

$$T_e - T_L = B\omega + \frac{J}{p}\frac{d\omega}{dt} \quad (14)$$

where Te is the electromagnetic torque, T_L is the load torque produced by the propeller, B is the coefficient of viscous friction, J is the moment of inertia.

In order to simulate the movement states of the aircraft. Following motion equation is added to the model of DSPMSM.

$$m\frac{dV_a}{dt} = F_t - F_d \quad (15)$$

where m is the weight of the aircraft. F_t is the thrust produce by propeller. F_d is the drag force which is the function of aircraft speed Va. $F_d = (\rho S C_d V_a^2)/2$. C_d is the drag coefficient and S is the cross-section area of aircraft [17].

2.3 Modelling of the propeller

According to the theoretical analysis of propeller, the characteristics of propeller are studied by momentum theory, blade element theory and eddy current theory [18]. An exact model of propeller can be built with the acknowledgement of all the necessary parameters, such as the velocity and pressure of the air. Nevertheless, it is difficult to observe the accurate value of these parameters in real time during simulation. To solve this problem, modelling with experimental method is widely applied in engineering [19-21]. As shown in equations (16)-(18), one can calculate thrust, input power and efficiency with thrust coefficient Ct, power coefficient Cp and other necessary parameters.

$$T = C_T \rho n^2 D^4 \quad (16)$$

$$P = C_P \rho n^3 D^5 \quad (17)$$

$$\eta = \frac{C_T}{C_P} J \quad (18)$$

where $J=Va/(n*D)$ is advance ratio,

ρ is air density(kg/m3),

n is propeller speed (revolution per second),

D is diameter of propeller (m),

Va is aircraft speed (m/s).

ISSN: 2414-1895 DOI: 10.6919/ICJE.202105_7(5).0060

Coefficient C_t and C_p are the functions of advanced ratio J and pitch angle β. These relationships are measured by National Advisory Committee for Aeronautics (NACA) in the 1930s for different propellers and relation curves were plotted in report No.464 [22]. The aerodynamic characteristics of propellers with different numbers of blades and aerofoil sections were compared and analysed. Most experiments consider only propeller characteristics in first quadrant while the report No.464 measured propeller characteristics in first and forth quadrant. It is beneficial for the modelling of propellers with two working modes. The thrust and power coefficient curves are plotted in Fig. 3 according to the experimental data from the report.

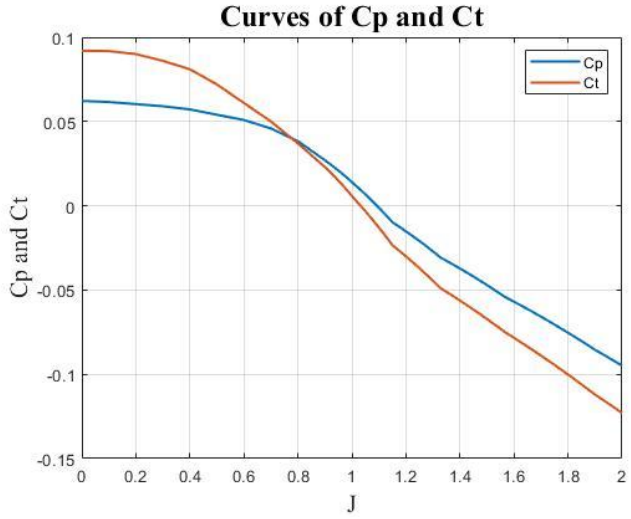

Figure 3. The thrust and power coefficient curves

Therefore, the propeller model is developed under the condition of known aircraft speed, air density, rotor speed and diameter of propeller. The Simulink model of propeller is shown in Fig. 4.

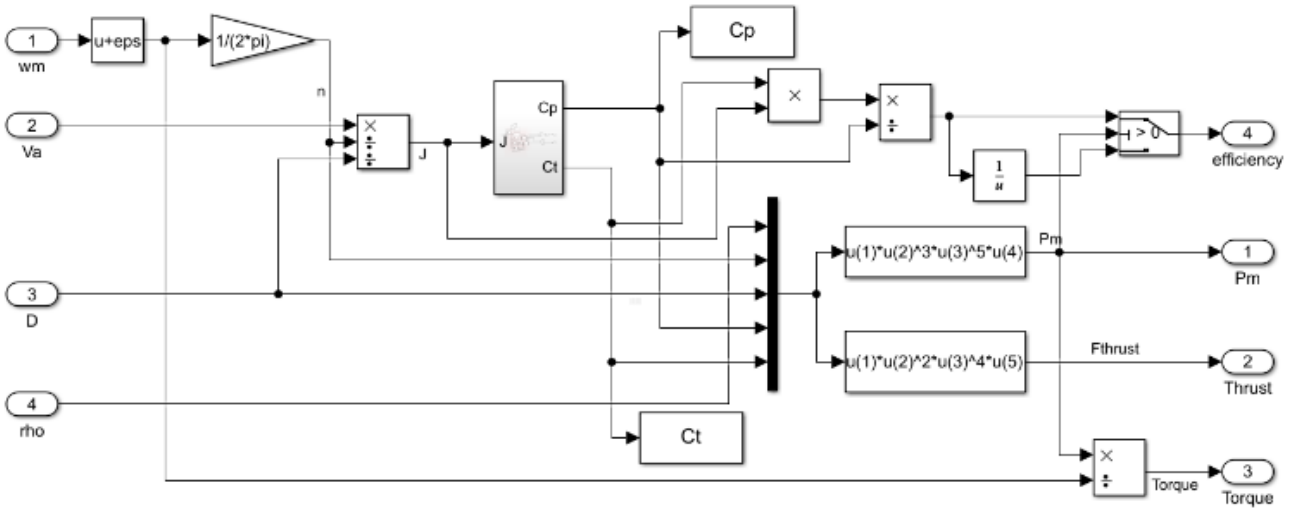

Figure 4. Model of propeller in MATLAB/Simulink.

3. Control scheme

3.1 Field oriented control

Field-oriented control (FOC) is a high-performance AC motor control method. This method is based on the coordinated transformation of stator variables (voltage, current and flux linkage). In the modelling of three-phase PMSM, three-phase static AC variables are transformed to two-phase

ISSN: 2414-1895 DOI: 10.6919/ICJE.202105_7(5).0060

rotating orthogonal DC variables. For example stator currents are decoupled into torque current,iq and flux excited current,id. By setting *d*-axis reference current to zero, electromagnetic torque only has relationship with *q*-axis current and permanent magnet flux linkage. So electromagnetic torque can be controlled by adjusting *q*-axis reference current for a fixed permanent magnet flux linkage. It ensures a good dynamic performance of PMSM like DC motor with FOC method. And the loss of the whole process can be reduced according to maximum torque per ampere (MTPA) strategy when i_d =0 strategy is applied to a mounted PMSM.

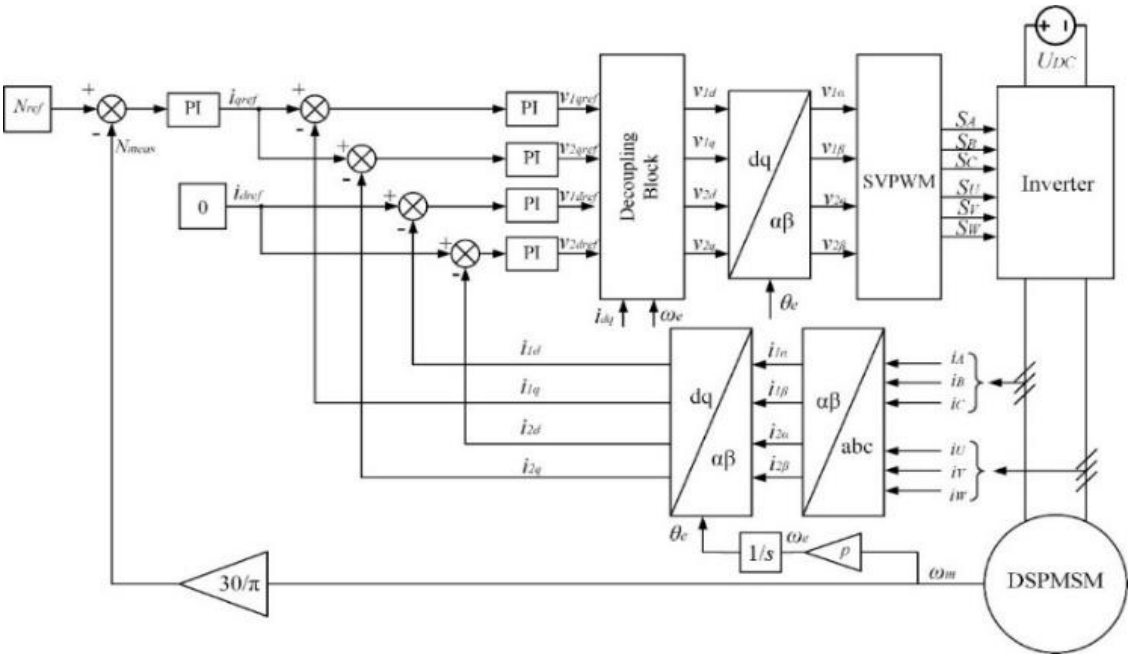

Figure 5. FOC system structure diagram for DSPMSM.

A FOC system structure diagram for DSPMSM is shown in Fig. 5. There are two loops in the control structure diagram. The inner loop is current loop, including d-axis and q-axis currents in two stators. The function of inner loop PI controller is to follow the reference current value which is calculated by speed loop controller. And the outer loop is speed loop accordingly. The rotor speed of DSPMSM is measured by sensor or calculated by sensorless control algorithm. Speed error generates q-axis reference current through speed PI controller. According to MTPA strategy, d-axis current is controlled to zero. In the inner loop, three-phase stator currents are measured and transformed into d-q rotating frame with the information of rotor position θ. Then the error signals of current are decoupled for better dynamic performance after regulating by the current PI controller. With inverse Park transformation, αβ axis voltages are used to generate switch signals for inverter with space vector pulse width modulation (SVPWM).

In normal conditions, the DSPMSM is working in the driving mode with positive rotating speed and electromagnetic torque. With velocity, current double closed loop control scheme, the rotating speed and torque of motor can be controlled accurately with short response time. FOC can also be applied in generator mode. According to load condition which is the working state of propeller in this study, the load torque may turn negative during the flight. Through FOC scheme, a negative q axis current can be demanded and electrical power flow through bi-direction convertor oppositely to the battery.

3.2 Maximum power point track algorithm in generator mode

During the landing process of a VLA, kinetic energy of propeller can be recovered to energy storage system (ESS) because of four quadrant operation characteristics of PMSM. When the rotor speed is positive while the electromagnetic torque is negative, PMSM is working in the regenerative braking mode. Regenerative braking control of PMSM based on field-oriented control is realised by requesting a negative q-axis current according to the braking toque demanded [14]. The propeller will

ISSN: 2414-1895 DOI: 10.6919/ICJE.202105_7(5).0060

act as a wind turbine. And the PMSM is actually a permanent magnet synchronous generator (PMSG) in this process.

In order to make the regenerative braking process more efficient, MPPT technique is applied in the control algorithm. Due to the instantaneous changing nature of the wind, it is essential to include a controller that can track the maximum peak regardless of wind speed [23].

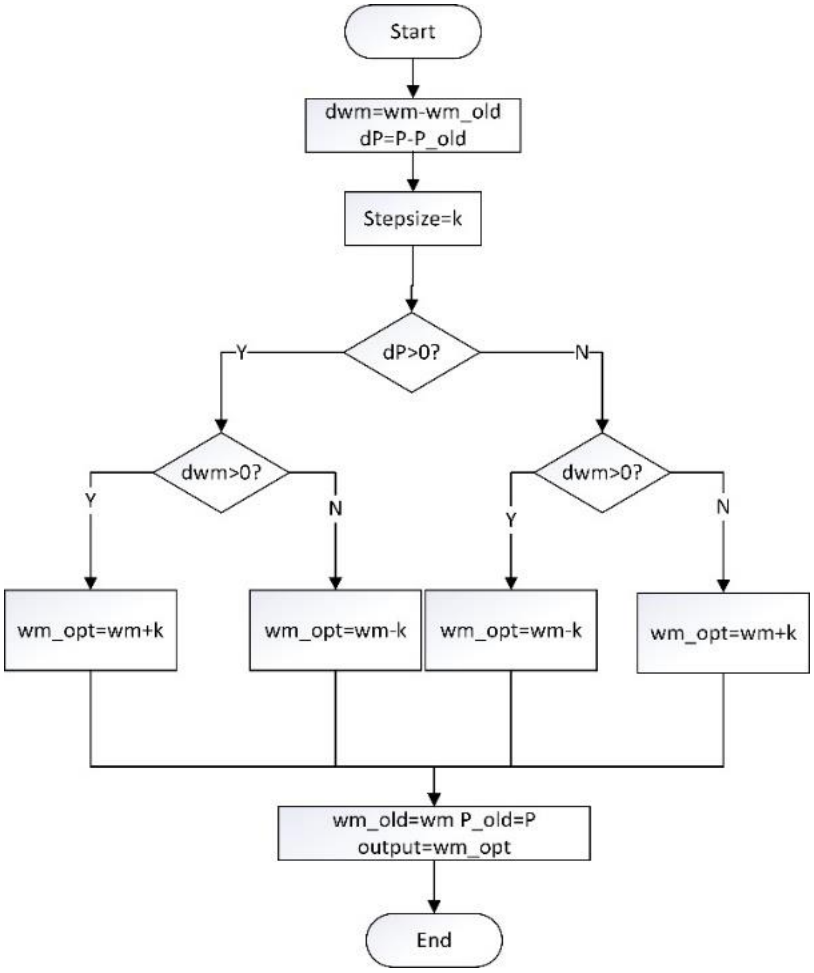

Figure 6. Flow chart of P&O MPPT algorithm

Among different kinds of MPPT algorithms, perturbation & observation (P&O) is adapted in this paper. Fig. 5 is the flow chart of P&O algorithm. The principle is to give the generator a small speed perturbation and detect the change of wind turbine output. Change the perturbation direction according to the variation of output power. Finally, the rotor speed will oscillate around optimal speed so that the mechanical power absorbed by generator can be maximized. The P&O method does not require prior knowledge of wind turbine mechanical characteristic which makes it independent and suitable for small scale system.

4. Simulation analysis and discussion

Performance of designed torque control system for DSPMSM based VLA has been verified through time-domain simulation using model (Fig. 5) build in MATLAB/Simulink. The basic parameters of electric propulsion system can be found in Appendix B Table 1. The simulation of EPS has been carried out in two different working conditions. Accordingly, the DSPMSM works in traction and generator mode respectively. In normal condition, propeller is consuming power produced by DSPMSM to drive the aircraft. The DSPMSM is working in traction mode during take-off and most time of cruise. The MPPT algorithm is inactive in this mode. While during landing phase, the load

ISSN: 2414-1895 DOI: 10.6919/ICJE.202105_7(5).0060

torque can be negative and propeller may produce a negative power which can be recovered by DSPMSM with P&O MPPT algorithm. The MPPT algorithm is active and keep tracking the optimum operating point of rotor speed when the working conditions of aircraft permits.

In traction mode, the initial value of rotor speed and aircraft velocity are all set zero. And a ramp speed reference is given to simulate the taking-off. As shown in Fig. 7(a), speed reference risen to 2800 rpm in 4.5 second. The motor can follow the speed reference with little overshoot and the static error is eliminated. Second figure is the d-q axis current of DSPMSM in the first stator. The second stator current is similar with that of first stator. The d axis current keeps nearly zero under the id = 0 method and q axis current has the similar shape with electromagnetic torque in forth figure which verifies the torque equation (16), the third figure presents the comparison between Pe and Pm, which are electrical power consumed by motor and the mechanical power applied to propeller. They keep increasing to 35 kW in 5 second and keeps almost constant. The velocity of aircraft is shown in the last figure.

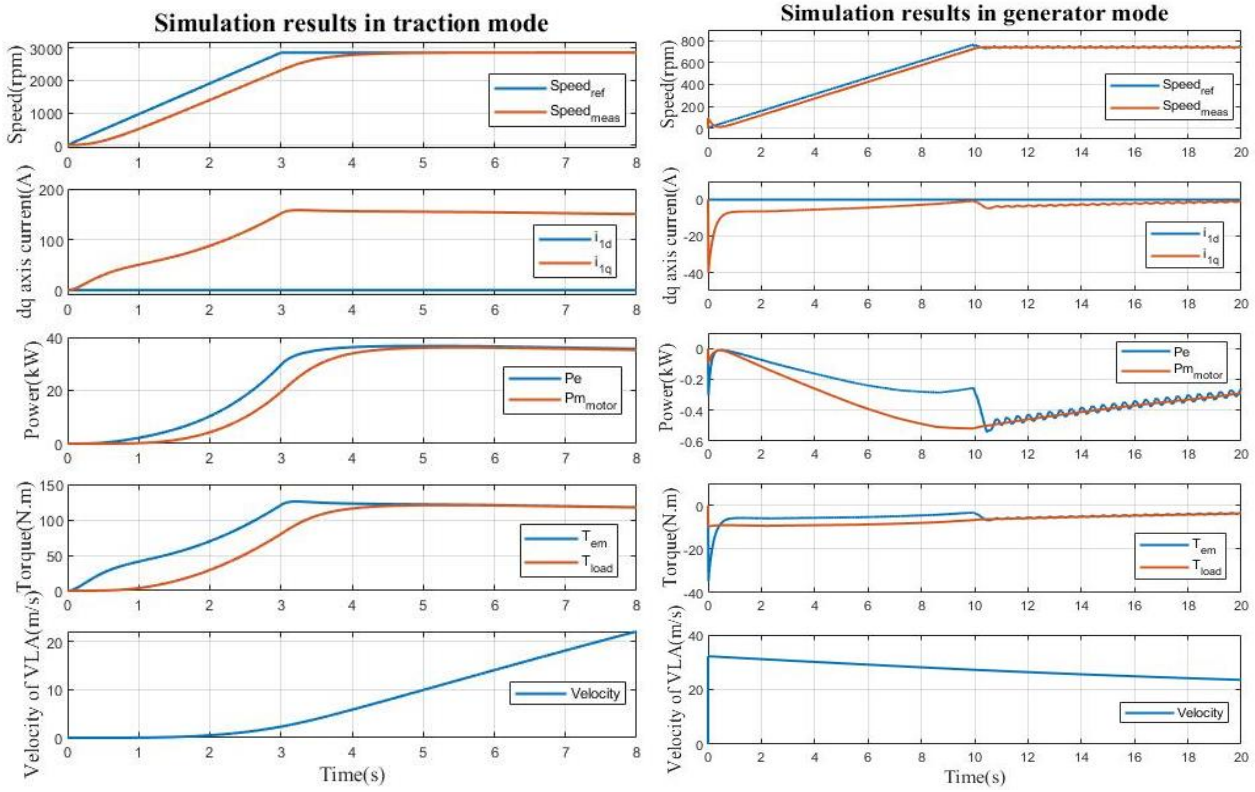

(a) (b)

Figure 7. Simulation results of EPS in traction mode(a) and generator mode(b)

In generator mode, the initial value of aircraft velocity is 32 m/s, and the rotor angular speed is 10 rad/s. The advance ratio J can be calculated and the working point of propeller is located in forth quadrant in this condition. According to the power and thrust coefficient curves shown in Fig. 3, propeller is producing negative power and torque. The kinetic energy is recycled from wind to the machine and battery during landing. The P&O MPPT algorithm is also enable in this stage. Simulation results in generator mode are shown in Fig. 7(b). The motor speed reference, the blue line, in the first figure is calculated by MPPT algorithm. And the measured motor speed, which is red line, can follow the speed reference very well. While some oscillation still can be found around optimum speed because the P&O algorithm is searching for the maximum power point. The second figure shows the current waveform of d and q axis in generator mode. Compared with the current in traction mode, q axis current became negative as expected. Thus, the DSPMSM produced a negative torque which is slightly smaller that load torque in absolute value as shown in forth figure. It means that the

ISSN: 2414-1895 DOI: 10.6919/ICJE.202105_7(5).0060

load torque of propeller is driving the motor as a generator in this mode. It also indicates negative mechanical and electrical power in the third figure. The electrical recovery power can reach a maximum value about 500W at 11 seconds. And the last figure is the aircraft velocity waveform. The speed is decreasing slowly because of the braking effect of the negative torque.

5. Conclusion

A double-stator PMSM based electric propulsion system for electric VLA has been built in the paper. The EPS can work both in traction and generator mode. The P&O MPPT algorithm is proposed to apply to the EPS in generator mode. Simulation results verified the rapidity and accuracy of DSPMSM under FOC scheme. And the effectiveness of MPPT algorithm during energy recovery has been confirmed in generator mode.

5.1 Appendix A

$$\boldsymbol{L_{s1}} = \begin{pmatrix} L_1 & M_1 & M_1 \\ M_1 & L_1 & M_1 \\ M_1 & M_1 & L_1 \end{pmatrix} + L_{12} \begin{pmatrix} cos\,2\,\theta_{s1} & cos(2\theta_{s1} - \frac{2\pi}{3}) & cos(2\theta_{s1} + \frac{2\pi}{3}) \\ cos(2\theta_{s1} - \frac{2\pi}{3}) & cos(2\theta_{s1} + \frac{2\pi}{3}) & cos\,2\,\theta_{s1} \\ cos(2\theta_{s1} + \frac{2\pi}{3}) & cos\,2\,\theta_{s1} & cos(2\theta_{s1} - \frac{2\pi}{3}) \end{pmatrix}$$

$$\boldsymbol{L_{s2}} = \begin{pmatrix} L_2 & M_2 & M_2 \\ M_2 & L_2 & M_2 \\ M_2 & M_2 & L_2 \end{pmatrix} + L_{22} \begin{pmatrix} cos\,2\,\theta_{s2} & cos(2\theta_{s2} - \frac{2\pi}{3}) & cos(2\theta_{s2} + \frac{2\pi}{3}) \\ cos(2\theta_{s2} - \frac{2\pi}{3}) & cos(2\theta_{s2} + \frac{2\pi}{3}) & cos\,2\,\theta_{s2} \\ cos(2\theta_{s2} + \frac{2\pi}{3}) & cos\,2\,\theta_{s2} & cos(2\theta_{s2} - \frac{2\pi}{3}) \end{pmatrix}$$

$$\boldsymbol{M_{s1s2}} = M_0 \begin{pmatrix} cos\,\gamma & cos(\gamma + \frac{2\pi}{3}) & cos(\gamma - \frac{2\pi}{3}) \\ cos(\gamma - \frac{2\pi}{3}) & cos\,\gamma & cos(\gamma + \frac{2\pi}{3}) \\ cos(\gamma + \frac{2\pi}{3}) & cos(\gamma - \frac{2\pi}{3}) & cos\,\gamma \end{pmatrix}$$

$$\boldsymbol{\psi_{m1}} = \psi_{sm1} \begin{pmatrix} cos\theta_{s1} \\ cos(\theta_{s1} - \frac{2\pi}{3}) \\ cos(\theta_{s1} + \frac{2\pi}{3}) \end{pmatrix}, \quad \boldsymbol{\psi_{m2}} = \psi_{sm2} \begin{pmatrix} cos\theta_{s2} \\ cos(\theta_{s2} - \frac{2\pi}{3}) \\ cos(\theta_{s2} + \frac{2\pi}{3}) \end{pmatrix}$$

5.2 Appendix B

Table 1. Parameters of propulsion system

Parameter	Mark	Value	Unit
Phase Resistance	R_s	8	mΩ
d-axis Inductance	L_{xd}	76	μH
q-axis Inductance	L_{xq}	79	μH
d-axis Mutual Inductance	M_d	5	μH
d-axis Mutual Inductance	M_q	5	μH
Rotor Inertia	J	0.0383	kg·m^2
Magnetic Flux Linkage	Ψ_{PM}	0.0355	Wb
Number of Pole Pair	p	10	/
Continuous/Maximal Current	/	160/340	A
Maximal Rotation Speed	/	5500	RPM
Voltage of DC Link	V_{dc}	500	V

ISSN: 2414-1895 DOI: 10.6919/ICJE.202105_7(5).0060

References

[1] Wenping Cao, B. C. Mecrow, G. J. Atkinson, J. W. Bennett, and D. J. Atkinson, 'Overview of Electric Motor Technologies Used for More Electric Aircraft (MEA)', IEEE Trans. Ind. Electron., vol. 59, no. 9, pp. 3523–3531, Sep. 2012, doi: 10.1109/TIE.2011.2165453.

[2] B. Sarlioglu and C. T. Morris, 'More Electric Aircraft: Review, Challenges, and Opportunities for Commercial Transport Aircraft', IEEE Transactions on Transportation Electrification, vol. 1, no. 1, pp. 54–64, Jun. 2015, doi: 10.1109/TTE.2015.2426499.

[3] A. Barzkar and M. Ghassemi, 'Electric Power Systems in More and All Electric Aircraft: A Review', IEEE Access, vol. 8, pp. 169314–169332, 2020, doi: 10.1109/ACCESS.2020.3024168.

[4] P. Wheeler, 'Technology for the more and all electric aircraft of the future', in 2016 IEEE International Conference on Automatica (ICA-ACCA), Oct. 2016, pp. 1–5, doi: 10.1109/ICA-ACCA.2016.7778519.

[5] M.-A. Shamsi-Nejad, B. Nahid-Mobarakeh, S. Pierfederici, and F. Meibody-Tabar, 'Fault Tolerant and Minimum Loss Control of Double-Star Synchronous Machines Under Open Phase Conditions', IEEE Transactions on Industrial Electronics, vol. 55, no. 5, pp. 1956–1965, May 2008, doi: 10.1109/ TIE.2008. 918485.

[6] T. Zhao, S. Wu, and S. Cui, 'Multiphase PMSM With Asymmetric Windings for More Electric Aircraft', IEEE Transactions on Transportation Electrification, vol. 6, no. 4, pp. 1592–1602, Dec. 2020, doi: 10.1109/ TTE.2020.2997609.

[7] E. Levi, 'Multiphase Electric Machines for Variable-Speed Applications', IEEE Transactions on Industrial Electronics, vol. 55, no. 5, pp. 1893–1909, May 2008, doi: 10.1109/TIE.2008.918488.

[8] Q. Zhu, A. Forsyth, and R. Todd, 'Investigation of Hybrid Electric Aircraft Operation on Battery Degradation', in 2018 IEEE International Conference on Electrical Systems for Aircraft, Railway, Ship Propulsion and Road Vehicles International Transportation Electrification Conference (ESARS-ITEC), Nov. 2018, pp. 1–6, doi: 10.1109/ESARS-ITEC.2018.8607617.

[9] S. Wu, C. Tian, W. Zhao, J. Zhou, and X. Zhang, 'Design and Analysis of an Integrated Modular Motor Drive for More Electric Aircraft', IEEE Transactions on Transportation Electrification, vol. 6, no. 4, pp. 1412–1420, Dec. 2020, doi: 10.1109/TTE.2020.2992901.

[10] H. Lin, H. Guo, and H. Qian, 'Design of High-Performance Permanent Magnet Synchronous Motor for Electric Aircraft Propulsion', in 2018 21st International Conference on Electrical Machines and Systems (ICEMS), Oct. 2018, pp. 174–179, doi: 10.23919/ICEMS.2018.8549030.

[11] A. Hebala et al., 'Feasibility Design Study of High-Performance, High-Power-Density Propulsion Motor for Middle-Range Electric Aircraft', in 2020 IEEE 29th International Symposium on Industrial Electronics (ISIE), Jun. 2020, pp. 300–306, doi: 10.1109/ISIE45063.2020.9152551.

[12] R. Alexander, D. Meyer, and J. Wang, 'A Comparison of Electric Vehicle Power Systems to Predict Architectures, Voltage Levels, Power Requirements, and Load Characteristics of the Future All-Electric Aircraft', in 2018 IEEE Transportation Electrification Conference and Expo (ITEC), Jun. 2018, pp. 194–200, doi: 10.1109/ITEC.2018.8450240.

[13] D. Lawhorn, V. Rallabandi, and D. M. Ionel, 'Electric Aircraft System Co-Simulation Including Body, Propeller, Propulsion, and Energy Storage Models', in 2019 IEEE Transportation Electrification Conference and Expo (ITEC), Jun. 2019, pp. 1–5, doi: 10.1109/ITEC.2019.8790529.

[14] V. Trifa, Gh. Brezeanu, and E. Ceuca, 'Analyzing the Efficiency of the Different Ways of Recovering Energy from a System Using a PMSM', in 2018 41st International Spring Seminar on Electronics Technology (ISSE), May 2018, pp. 1–4, doi: 10.1109/ISSE.2018.8443706.

[15] L. Fan, T. Yang, M. Rashed, and S. Bozhko, 'Sensorless control of dual-three phase PMSM based aircraft electric starter/generator system using model reference adaptive system method', in CSAA/IET International Conference on Aircraft Utility Systems (AUS 2018), Jun. 2018, pp. 787–794, doi: 10.1049/cp.2018.0138.

[16] J. Karttunen, S. Kallio, P. Peltoniemi, P. Silventoinen, and O. Pyrhönen, 'Dual three-phase permanent magnet synchronous machine supplied by two independent voltage source inverters', in Automation and Motion International Symposium on Power Electronics Power Electronics, Electrical Drives, Jun. 2012, pp. 741–747, doi: 10.1109/SPEEDAM.2012.6264448.

ISSN: 2414-1895 DOI: 10.6919/ICJE.202105_7(5).0060

[17] P. Guarino, G. L. Cascella, and S. Stasi, 'Multiobjective Optimization for Electric Drives Design in Solar-Powered Ultralight Aircrafts', p. 7.

[18] B. W. McCormick, Aerodynamics, aeronautics, and flight mechanics, 2nd ed. New York: Wiley, 1995.

[19] E. P. Hartman and D. Biermann, 'The Aerodynamic Characteristics of Full-Scale Propellers Having 2, 3, and 4 Blades of Clark Y and R.A.F. 6 Airfoil Sections', Jan. 1938, Accessed: Jun. 20, 2020. [Online]. Available: http://ntrs.nasa.gov/search.jsp?R=19930091715.

[20] A. M. Kamal, A. Bayoumy Aly, and A. Elshabka, 'Modeling and Simulation of Propeller Propulsion Model Using Wind Tunnel', Jan. 2015, doi: 10.2514/6.2015-1596.

[21] K. Takahashi, H. Fujimoto, Y. Hori, H. Kobayashi, and A. Nishizawa, 'Modeling of propeller electric airplane and thrust control using advantage of electric motor', in 2014 IEEE 13th International Workshop on Advanced Motion Control (AMC), Mar. 2014, pp. 482–487, doi: 10.1109/AMC.2014.6823329.

[22] E. P. Hartman, 'Negative Thrust and Torque Characteristics of an Adjustable-Pitch Metal Propeller', UNT Digital Library, May 23, 1933. https://digital.library.unt.edu/ark:/67531/metadc66121/ (accessed Feb. 27, 2021).

[23] M. A. Abdullah, A. H. M. Yatim, C. W. Tan, and R. Saidur, 'A review of maximum power point tracking algorithms for wind energy systems', Renewable and Sustainable Energy Reviews, vol. 16, no. 5, pp. 3220–3227, Jun. 2012, doi: 10.1016/j.rser.2012.02.016.